Engenharia Agrícola
ISSN: 1809-4430 (online)
www.engenhariaagricola.org.br | www.scielo.br/j/eagri

Scientific Paper
DOI: http://dx.doi.org/10.1590/1809-4430-Eng.Agric.v45e20240212/2025

DEVELOPMENT OF AN LADRC-BASED TILLAGE DEPTH CONTROL SYSTEM FOR ELECTRIC ROTARY TILLER

Bin Chen [1,2], Wei Tao[1,2*], Xinkun Yang[1], Shaoye Ke[1], Shenghong Huang[1]

[2*]Corresponding author. Fujian Key Laboratory of Big Data Application and Intellectualization for Tea Industry, Wuyi University, Nanping, Fujian, China. E-mail: taowei@wuyiu.edu.cn | ORCID ID: https://orcid.org/0000-0002-7281-6776

KEYWORDS

tea plantations, LADRC, electric rotary tiller, tillage depth control, field experiments.

ABSTRACT

Precision control of tillage depth is crucial for optimizing soil preparation in tea plantations. This study presents an adaptive real-time tillage depth control system based on Linear Active Disturbance Rejection Control (LADRC) to address precision challenges in the tillage depth of electric rotary tillers in tea plantations. The system, constructed using body posture sensors, control units, and hybrid stepper motors, integrates sensor data and LADRC technology to drive the stepper motor, enabling precise tillage depth control. The displacement sensor signals were collected, and the actual tillage depth was compared with the target values, allowing adjustments to achieve closed-loop control of the rotary tiller. Field experiments at speeds of 0.5 km/h and 0.8 km/h with tillage depths of 80 mm and 100 mm demonstrate the system's effectiveness. The LADRC system achieved a standard deviation of 3.2 mm, outperforming fuzzy PID (10.5 mm) and sliding mode control (5.9 mm). The rate of depth variation was reduced by 44.8% and 68.9% compared to the fuzzy Proportional Integral Derivative (PID) and SMC, respectively. These results confirm that the LADRC-based system effectively minimizes interference during rotary-tiller operation, ensuring the stability and reliability of tillage depth control.

INTRODUCTION

The advancement of modern agricultural technology has significantly improved mechanized farming operations. Electric rotary tillers are important agricultural tillage machines that play a critical role in enhancing the efficiency and quality of tillage operations (Liu et al., 2024a; Sahoo & Raheman, 2020). One of the key challenges in achieving high-quality tillage is tillage depth control, as it directly affects soil turnover, crop planting depth, and soil-seeds contact, all of which affects crop growth and yield (Fawzi et al., 2021). However, traditional tillage depth control methods rely on manual adjustments, which are often imprecise and slow, making them unsuitable for precision requirements of modern agriculture. To overcome these challenges, intelligent control systems have been integrated into electric rotary tillers, enabling real-time monitoring and dynamic depth adjustment to enhance operational quality and efficiency (Kim et al., 2022; Wang et al., 2024).

Current research on automated tillage depth control primarily focuses on improving tillage depth regulation (Liu et al., 2023a; Liu et al., 2024b). Various methods have been explored, such as fuzzy proportional-integral-derivative (PID) control, high-precision monitoring models, and sliding mode control (SMC) algorithms. Xiao et al. 2023 proposed a novel fuzzy PID control strategy to improve response speed and operational accuracy in a self-propelled electric mini-tiller. Similarly, Hu et al. (2024) developed a high-precision monitoring model using model identification techniques to optimize control functions. A fuzzy adaptive PID method was employed to adjust the tillage depth, enhancing system response speed and anti-interference capability (Hu et al., 2024). Wang et al. (2023) introduced a sliding mode control algorithm to regulate speed and slip

[1] The Key Laboratory for Agricultural Machinery Intelligent Control and Manufacturing of Fujian Education Institutions, Wuyi University, Nanping, Fujian, China.
[2] Fujian Key Laboratory of Big Data Application and Intellectualization for Tea Industry, Wuyi University, Nanping, Fujian, China.

Area Editor: João Paulo Arantes Rodrigues da Cunha
Received in: 10-26-2024
Accepted in: 2-10-2025

ratio, reducing tillage depth errors and enhancing uniformity. Additionally, an improved tillage depth control strategy for complex farmland terrain using mechanical angle sensors to precisely measure the hydraulic lift arm angle, correlating it with the tillage angle for high-precision control. The Hybrid Extended State Observer Back Stepping Sliding Mode controller (HESO-Back Stepping SMC) provides continuous and smooth control signals while reducing chattering, demonstrating its effectiveness in complex agricultural environments (Wang et al., 2024). Furthermore, Kim et al. (2020) designed a real-time tillage depth measurement system that integrates sensor fusion methods, allowing for accurate tillage depth monitoring synchronized with traction force measurement data from ASABE standard equations.

Despite this, existing control methods still face challenges in optimizing response speed, reducing interference, and maintaining tillage depth precision in variable agricultural environments (Hu et al., 2024; Jia et al., 2016; Luo et al., 2023; Sabouri et al., 2021). Most research teams have focused on traditional field operations, where rotary tillers rely heavily on hydraulic actuators and conventional control techniques (Hu et al., 2024; Jia et al., 2016; Luo et al., 2023; Sabouri et al., 2021). However, significant gaps remain in the development of automated tillage systems tailored for specialized environments such as tea gardens. Ensuring consistent tillage depth accuracy, uniform tillage across varying terrains, and reliable sensor fusion data remains a challenge. The unique soil structure and crop arrangements in tea gardens require adaptive control strategies, which conventional tillage methods fail to provide due to their limitations in response speed, anti-interference capability, and overall precision.

To address these challenges, this study proposes an adaptive real-time tillage depth control system based on Linear Active Disturbance Rejection Control (LADRC). The system integrates posture sensors, hybrid stepper motors, an extended Kalman filter for noise, and a grating sensor for real-time monitoring and correction. Unlike conventional control systems, LADRC provides superior disturbance rejection, enabling precise tillage control even in variable environmental conditions. This study is the first to propose a LADRC-based, rotary tilling system specifically designed for tea gardens, ensuring high plowing accuracy while improving response time, stability, and adaptability to soil variations. By addressing sensor fusion, terrain irregularity, and interference effects, this study contributes to the development of precision agriculture, offering an innovative and reliable solution for intelligent tillage depth control in specialized agricultural settings.

Structure and working principle of the electric rotary tiller

The overall configuration of the electric rotary tiller is illustrated in Figure 1. The system comprises three primary components: a walking mechanism, a working mechanism, and an electrical control system. The walking mechanism consists primarily of the body of an electric rotary tiller. The working mechanism, positioned at the front, includes a rotary tiller mounted on a lead-screw sliding table. The electrical control system included a hybrid stepper motor, lead screw sliding table, rotary-tiller lift controller, electric-tiller walking controller, and rotary-tiller motor.

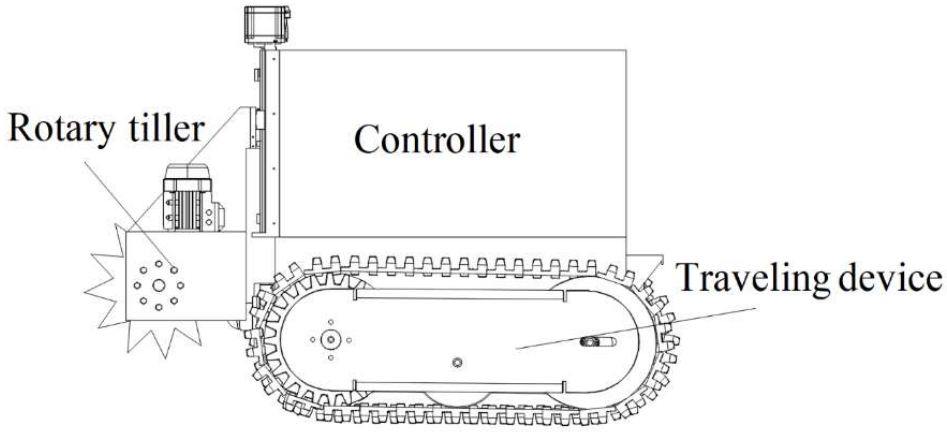

FIGURE 1. Overall structural diagram of the electric tiller.

The adaptive real-time tillage depth control system comprises three principal units: a rotary tiller posture sensor, a control unit, and a hybrid stepper motor lead-screw sliding table. A rotary-tiller posture sensor is principally employed to detects variations in the posture of the rotary tiller when the electric rotary tiller traverses an uneven road. The control unit employs an STM32F407 control chip, wherein the microprocessor incorporates the input data from the sensors and executes extended Kalman filtering and predictive processing. The LADRC then processes the data and generates the required pulse-control signals for transmission to the hybrid stepper motor driver. The hybrid stepper motor lead screw sliding table was responsible for driving the upward and downward movements of the rotary tiller blade. Signals indicating the real-time tillage depth are transmitted by the grating sensor to the control unit, thereby completing the adaptive real-time tillage depth control process. The adaptive real-time tillage depth control system ensures precise rotary tillage depth through the following steps, as illustrated in Figure 2.

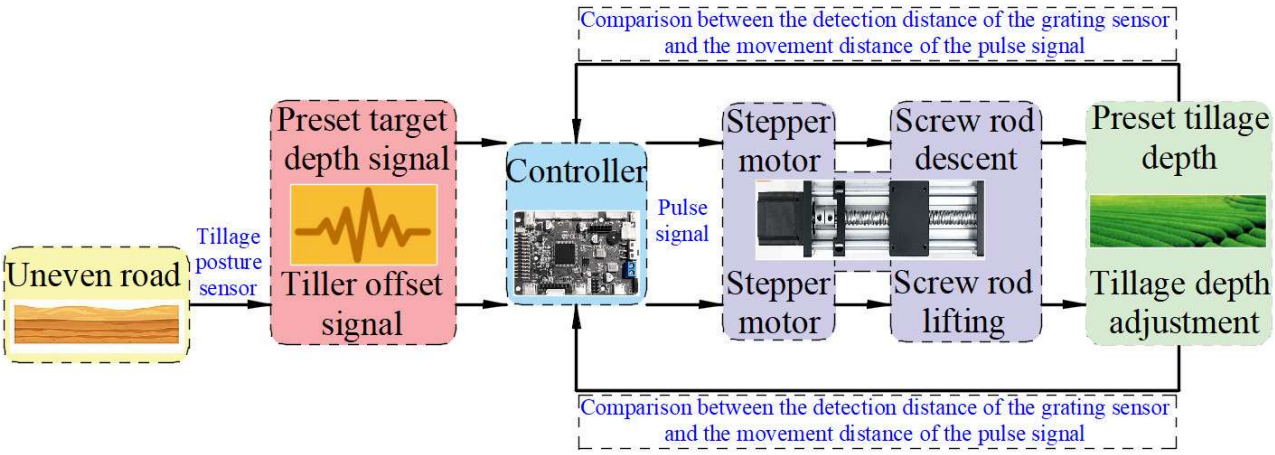

FIGURE 2. Tillage Depth Control System Workflow.

The control unit receives the preset target tillage depth remotely via wireless communication. This data is then transmitted to the rotary-tiller control system, which calculates and sends pulse signals to the hybrid stepper motor. The lead-screw sliding table then descends to the designated depth. The grating sensor, mounted on the guide rail, continuously monitors the displacement of the lead screw in real time and compares it with the preset tillage depth signal. This ensured that the desired depth was accurately maintained. In the event of an uneven working environment, the control unit utilizes signals from the rotary-tiller posture sensor. It performs extended Kalman filter preprocessing to handle external disturbances such as vibrations and body deviations while the electric rotary tiller is in motion. The control unit calculates the necessary adjustments, converts them into pulse signals, and transmits them to the hybrid stepper motor, which drives the lead-screw sliding table. This process regulates the ascent and descent of the rotary tiller, ensuring it remains stable at the desired position. Once the hybrid stepper motor completes the lifting movement, the control unit collects displacement signals from the grating sensor in real time, providing an accurate measurement of the tillage depth. By continuously comparing the actual tillage depth signals with the preset values, the control unit adapts and corrects errors using the LADRC algorithm. This forms a complete closed-loop control process that ensures the precision and stability of the tillage depth.

Real-time adaptive tillage depth control method

Tillage depth automatic control system and method

Traditional tillage-depth control methods rely on position-based adjustment and force-based adjustment, each with advantages and limitations. Force-based adjustment is less affected by terrain fluctuations, but it is prone to errors in real-time soil resistance detection, leading to inconsistent tillage depth. Conversely, position-based adjustment is not affected by soil resistance, and it can introduce significant errors when terrain fluctuations are severe. In such cases, additional sensors are required to correct inaccuracies. In general, two primary tillage-depth control methods are used: switch-based adjustment and control coefficients. The control coefficient method, which utilizes parameters derived from extensive research and practical experience, can achieve superior control performance. Given the relatively stable terrain conditions under which electric rotary tillers are deployed in tea plantations, position-based adjustment offers a clear advantage.

Considering the factors mentioned above, this study employs a combined measurement method using posture and grating sensors. This significantly reduces vibrations and external disturbances in the electric rotary tiller. The LADRC controller was integrated to further minimize errors, and a hybrid stepper motor mechanism was used to ensure stable and precise tillage depth control. The rotary tiller posture sensor detects surface unevenness in real-time, and the data were preprocessed using the extended Kalman filter algorithm. To minimize redundancy and reliability, attitude sensors are designed with both main and backup configurations. The preset tillage depth is continuously compared with the actual depth to determine the requisite real-time adjustment, which was computed by the LADRC and converted into pulse-control signals to drive the stepper motor. The grating sensor continuously monitors tillage depth in real time, delivering feedback to the LADRC controller, which further facilitates adaptive adjustment of the tiller depth in real time. The sensor installation locations are shown in Figure 3, while Figure 4 illustrates the control system schematic.

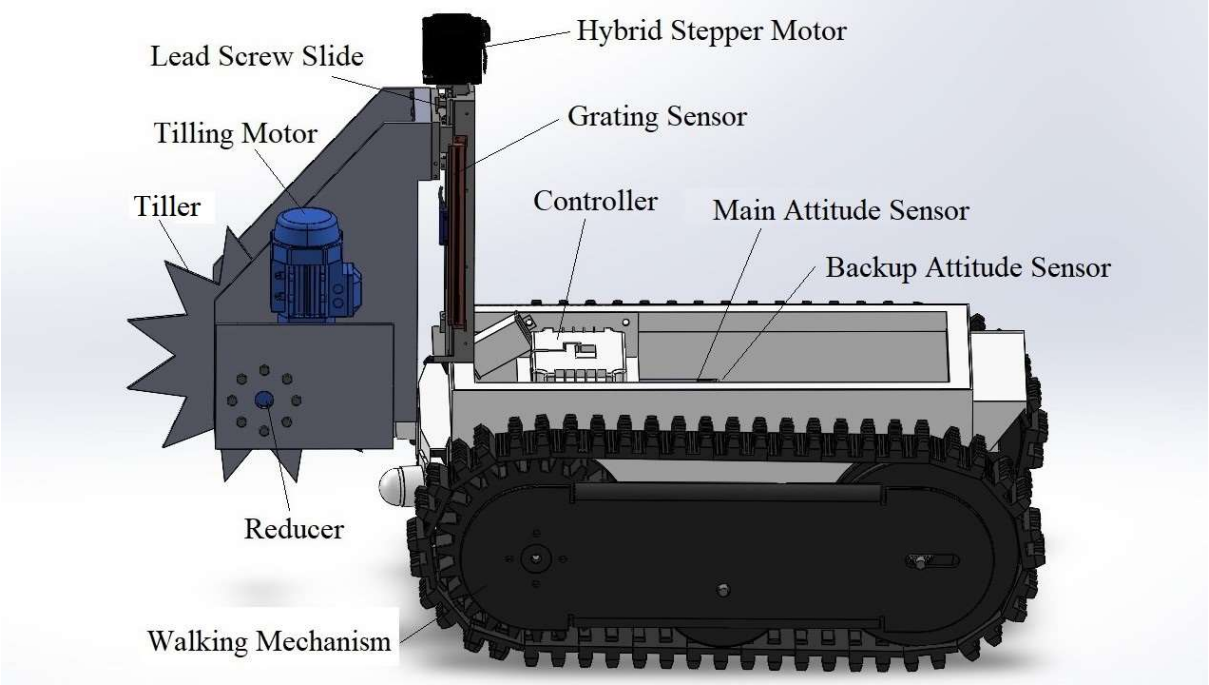

FIGURE 3. Schematic diagram of automatic tillage depth control system.

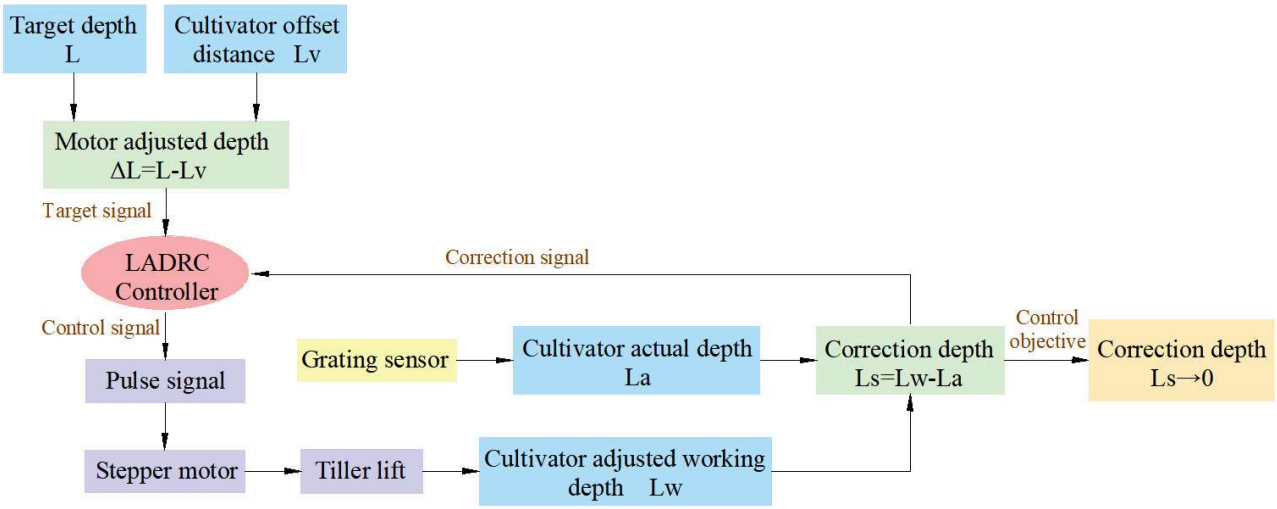

FIGURE 4. LADRC Regulation Principle Diagram.

A hybrid stepper motor is an open-loop control device that converts electrical pulse signals into angular or linear displacements. The motor's speed and stopping position were determined entirely by the frequency and number of the pulse signals. Each received pulse signal prompts the stepper driver to rotate the motor by a predetermined angle in the designated direction. The main parameters of the stepper motor were calculated as follows:

$$\begin{cases} \theta = \dfrac{360}{N} \times K_0 \\ l = \dfrac{\theta \times \mathrm{P}}{360} \\ n = 60 \times f \\ v = \dfrac{\mathrm{n} \times P}{360} \times 60 = f \times P \end{cases} \quad (1)$$

Where:

θ' is the step angle (°);

N is the number of steps of the stepper motor (related to the motor driver);

θ is the motor's working rotation angle (°);

K_0 is the number of pulses, l is the stroke of the sliding table (mm);

P is the lead screw pitch (mm);

n is the motor speed (rpm), and v is the sliding table movement speed (mm/s).

When an electric rotary tiller encounters an uneven road, it may experience positional shifts during its operation. The controller made real-time adjustments to the stepper motor based on the position changes detected by the posture sensor, thereby enabling the system to adapt to alterations in the direction of the tillage depth.

$$\Delta K = \frac{360 \times \Delta L}{\theta' \times P} = \frac{\Delta L \times N}{P} \quad (2)$$

Where:

ΔK represents the number of altered pulse signals, and

ΔL represents the actual adjusted tillage depth achieved by the stepper motor (which can be obtained from the pitch and roll angle deviations detected by the tillage depth posture sensor and calculated accordingly). Once the stepper motor has been adjusted in accordance with ΔK, the actual working depth of the rotary tiller is assumed to be L_w, while the actual depth detected by the grating sensor is L_a. Subsequently, the real-time adjustment error in the tillage depth can be obtained, as shown in [eq. (3)].

$$L_s = L_w - L_a \quad (3)$$

The use of a feedback controller to correct the rotary tiller depth in real-time allows the shortest possible approach to zero for L_s. This method, which adjusts the tillage depth in real-time according to surface irregularities, has been shown to be highly effective in farming environments where terrain changes are minimal. A posture sensor on a rotary tiller can measure the surface unevenness of a tillage environment in real-time. Assuming the initial pitch angle is α, and the detected pitch angle at the next moment is α', the distance between the center of gravity O of the tiller and the center of gravity P of the rotary tiller is x, as illustrated in Figure 5.

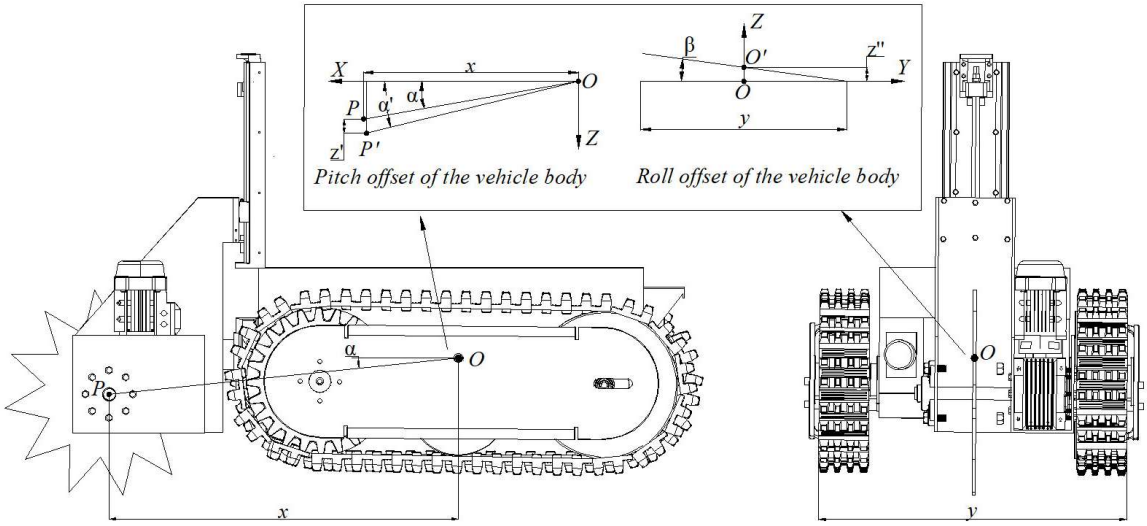

FIGURE 5. Geometric plot of tillage depth versus attitude angle.

The change in the rotary tiller depth z' after the modification of the pitch angle can be calculated in accordance with the principles of geometry, as illustrated in [eq. (4)].

$$z' = \frac{x}{cos\alpha} \times sin\alpha' - x \times tan\alpha \quad (4)$$

In addition to the effect of the pitch angle on changes in the rotary-tiller depth, the roll angle also exerts an influence on the tillage depth, as illustrated in Figure 5. The impact of a modification in roll angle on the rotary tiller depth is represented by z'', as illustrated in [eq. (5)].

$$z'' = \frac{y}{2} \times tan\beta \quad (5)$$

Where:

y is the width of the electric rotary tiller, and

β is the roll angle measured by the posture sensor. By combining eqs (4) and (5), the real-time tillage depth variation ΔL of the electric rotary tiller can be obtained, as demonstrated by the following equation:

$$\Delta L = z' + z'' \quad (6)$$

Dynamic model of the hybrid stepper motor

The two-phase hybrid stepper motor described in this study consists of a stator and a rotor. The magnetic poles of the stator generate a magnetic field that attracts the rotor's poles, thereby causing the rotor's magnetic field to rotate in synchrony with the stator's magnetic field (Groenhuis et al., 2021; Li et al., 2023). Both the stator and rotor are composed of permanent magnets. The stator comprised eight evenly distributed magnetic poles arranged in two distinct phases. Each phase contains four poles, resulting in a total of eight poles distributed across the stator (Wu et al., 2020). In formulating the mathematical model of the stepper motor, the leakage flux between the stator poles and the permanent magnet of the rotor was neglected, along with the effects of hysteresis, eddy currents, and harmonic components induced in the stator coils. A mathematical model for each phase was constructed based on an electromagnetic circuit model. This is shown in Fig. 6.

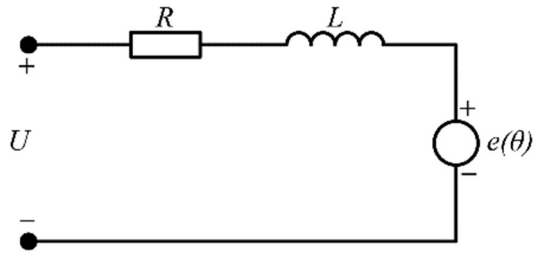

FIGURE 6. Single-phase equivalent circuit for two-phase hybrid stepper motor.

The pulse input signal is denoted as θ_i, and upon receiving this signal, the stepper motor rotates with an actual rotation angle being θ_o. The voltage balance equation for the two-phase hybrid stepper motor is (Hojati et al., 2024):

$$\begin{cases} U_a = Ri_a + L\frac{di_a}{dt} - K_m\omega\sin(Z_r\theta) \\ U_b = Ri_b + L\frac{di_b}{dt} + K_m\omega\sin(Z_r\theta) \\ T_E = J\frac{d\omega}{dt} + B\omega + T_L = -K_m i_a\sin(Z_r\theta) + K_m i_b\cos(Z_r\theta) \end{cases} \quad (7)$$

Where:

U_a and U_b represent the phase voltages of the two-phase windings and i_a and i_b denote the currents of the two-phase windings. L signifies the average self-inductance, and θ represents the angular displacement of the stepper motor. R represents the phase resistance of the two-phase windings. In this context, J represents the moment of inertia, and B is the viscous damping coefficient, T_E is the electromagnetic torque, T_L is the load torque, Z_r is the number of teeth in the stepper motor, and K_m is the stepper motor constant. In accordance with [eq. (7)] and the dynamic characteristics of the stepper motor, when a single-phase excitation is considered as a case study, and the load torque is assumed to be zero, the following can be derived by energizing the motor:

$$J\frac{d^2\theta}{d^2t} + B\frac{d\theta}{dt} - \frac{Z_r L i_a^2}{2}\sin(Z_r\theta) = 0 \quad (8)$$

Initially, the stepper motor was in equilibrium, and the rate of change in the stepper angle was approximately zero. Thus, the equation of motion for the stepper-angle increment can be expressed as follows:

$$J\frac{d^2(\delta\theta)}{d^2t} + B\frac{d(\delta\theta)}{dt} - \frac{Z_r L i_a^2}{2}\sin[Z_r(\delta\theta)] = 0 \quad (9)$$

Where:

$\delta\theta$ is the angular increment, which can be expressed as $\delta\theta = \theta_0 - \theta_i$. Given that $\delta\theta$ is exceedingly small, its linearized infinitesimal polarity can be derived.

$$J\frac{d^2\theta_o}{d^2t} + B\frac{d\theta_o}{dt} + \frac{Z_r^2 L i_a^2}{2}\theta_o = \frac{Z_r^2 L i_a^2}{2}\theta_i \quad (10)$$

The Laplace transform can be applied to both sides of [eq. (10)] simultaneously, with the initial value set to zero to yield

$$(Js^2 + Bs + \frac{Z_r^2 L i_a^2}{2})\theta_o(s) = \frac{Z_r^2 L i_a^2}{2}\theta_i(s) \quad (11)$$

The transfer function of the two-phase hybrid stepper motor is expressed as

$$G(s) = \frac{\theta_o(s)}{\theta_i(s)} = \frac{\frac{Z_r^2 L i_a^2}{2J}}{s^2 + \frac{B}{J}s + \frac{Z_r^2 L i_a^2}{2J}} \quad (12)$$

The hybrid stepper motor parameters used in this study are listed in Table 1.

TABLE 1. Primary characteristics of the hybrid stepper motor.

Parameters	Values
Number of teeth Z_r	50
Phase current i_a/A	3
Viscous damping coefficient B	0.03
Rotor inertia $J/kg*cm^2$	0.365
Phase inductance L/mH	3.70

By substituting the parameters mentioned above into the transfer function in [eq. (12)], the result is as follows:

$$G(s) = \frac{228.08}{s^2 + 0.08s + 228.08} \quad (13)$$

Design of the adaptive ADRC controller for tillage depth

In 1999, Jingqing Han proposed an advanced control strategy known as Active Disturbance Rejection Control (ADRC) (Han, 1999). The fundamental premise of this approach is to conceptualize the inherent uncertainties of the system, both internal and external, as a unified disturbance. This disturbance was then estimated and compensated using an Extended State Observer (ESO). The core structure of the ADRC consists of three key components: the Tracking Differentiator (TD), Extended State Observer (ESO), and Nonlinear State Error Feedback (NLSEF) control law. The TD extracts a continuous signal and its derivative from the system input, whereas the ESO estimates the system state and overall disturbance. Based on the output of the ESO, the NLSEF formulates a control law that facilitates the precise control of the system state (Han, 2009). The fundamental configuration is illustrated in Figure 7.

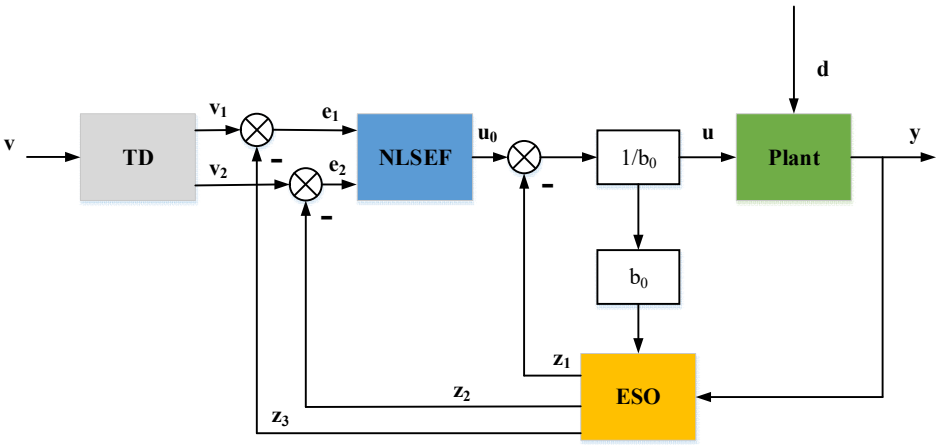

FIGURE 7. The basic structure of the ADRC.

In this context, the variable "*v*" represents the input signal, "*d*" represents the total external disturbance, and "*y*" represents the actual output.

Given the nonlinear nature of NLSEF and the associated difficulties in analyzing them in practical applications, they are frequently replaced by linear active disturbance rejection controls (LADRCs) in engineering. Gao et al. further refined and optimized the LADRC by employing linear gains instead of nonlinear gains, thereby streamlining the implementation and adjustment of the control algorithm (Gao, 2003; Gao et al., 2024). A simplified LADRC structure is shown in Fig. 8.

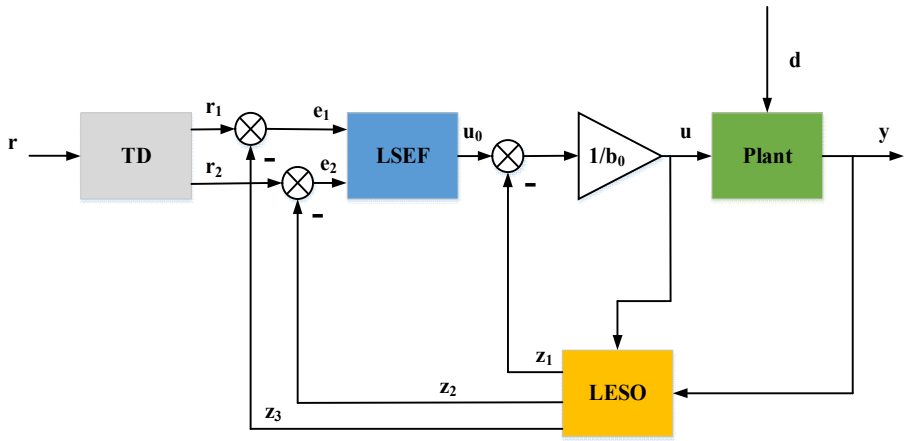

FIGURE 8. The basic structure of the LADRC.

In this context, the variable "*r*" represents the input signal for the LADRC. As illustrated in the basic structural diagram of the LADRC, the TD, LESO, and LSEF components operate in concert to effectively regulate the system. The TD component defines the desired dynamic behavior, the LESO component provides real-time estimates of the system state, and the LSEF component generates appropriate control signals based on this information, thereby achieving precise control of the system dynamics. This method is particularly well-suited to systems exhibiting unknown or evolving dynamics, as it does not necessitate the use of an accurate system model.

As illustrated in [eq. (13)], the control object for the electric rotary tiller can be identified as a second-order model. Accordingly, the LADRC for a second-order object can be designed as follows.

$$\ddot{y} = -a_1\dot{y} - a_2 y + w + bu \tag{14}$$

In [eq. (14)], u represents the system input, y denotes the output, w signifies the external disturbance, a_1 and a_2 are the system parameters, and b is the control gain. The parameters a_1, a_2, and b are unknown, with $b_0 \approx b$. Let $x_1 = y$ and $x_2 = \dot{y}$. The following assumptions were made.

$$f(y, \dot{y}, w) = -a_1\dot{y} - a_2 y + w + (b - b_0)u \tag{15}$$

Equation (15) defines the generalized disturbance of the system, which includes both internal and external uncertainties. It is expanded into the state variable of the system, $x_3 = f(y, \dot{y}, w)$, from which the state equation of (16) is derived.

$$\begin{cases} \dot{x}_1 = x_2 \\ \dot{x}_2 = x_3 + b_0 u \\ \dot{x}_3 = h \\ y = x_1 \end{cases} \tag{16}$$

Where:

x_1, x_2, and x_3 represent the system state variables, and h is defined as $\dot{f}(y, \dot{y}, w)$. In light of the considerations mentioned above, a linear extended state observer (LESO) is thus established.

$$\begin{cases} \dot{z}_1 = z_2 - \beta_1(z_1 - y) \\ \dot{z}_2 = z_3 - \beta_2(z_1 - y) + b_0 u \\ \dot{z}_3 = -\beta_3(z_1 - y) \end{cases} \quad (17)$$

By selecting appropriate observer gains β_1, β_2, and β_3, the LESO is capable of achieving real-time tracking of each variable in [eq. (14)], that is to say, $z_1 \to y$, $z_2 \to \dot{y}$, $z_3 \to f(y, \dot{y}, w)$. Let u be defined as follows: $u = \frac{-z_3 + u_0}{b_0}$. Furthermore, let us neglect the estimation error of z_3 on $f(y, \dot{y}, w)$. In this case, (14) can be simplified to a double-integrator cascade structure.

$$\ddot{y} = (f(y, \dot{y}, w) - z_3) + u_0 \approx u_0 \quad (18)$$

Design of the PD controller:

$$u_0 = k_p(v - z_1) - k_d z_2 \quad (19)$$

Where:

v represents the reference signal, while k_p and k_d denote the controller gains. The closed-loop transfer function of the system can be derived in accordance with the principles set forth in eqs (18) and (19).

$$G_{cl}(s) = \frac{k_p|}{s^2 + k_d s + k_p} \quad (20)$$

An appropriate selection of the gains (k_p and k_d) can stabilize the system. The characteristic equation of LESO is as follows:

$$\lambda(s) = s^3 + \beta_1 s^2 + \beta_2 s + \beta_3 \quad (21)$$

By selecting the optimal characteristic equation, $\lambda(s) = (s + \omega_o)^3$, the result is:

$$\beta_1 = 3\omega_o, \beta_2 = 3\omega_o^2, \beta_3 = \omega_o^3 \quad (22)$$

In this equation, the term ω_o is defined as the observer bandwidth. Similarly, the parameters in Eq. (20) can be selected as follows:

$$k_p = \omega_c^2, k_d = 2\xi\omega_c \quad (23)$$

In the [eq. (23)], ω_c is represents the controller bandwidth, while ξ represents the damping ratio. When the value of ξ is set to 1, the LADRC control parameters configuration simplifies to selecting three key parameters: the observer bandwidth ω_o, the controller bandwidth ω_c, and the control gain b_0. This significantly simplifies the complexity of controller-parameter configuration.

The principal function of the LADRC is to transform the feedback data from the grating sensor into pulse control signals that regulate the operation of the stepper motor. This conversion process is crucial for achieving the precise control of real-time adaptive tilling-depth systems. During operation, the grating sensor continuously monitors the actual tillage depth of the rotary tiller and generates the corresponding measurements. Subsequently, the measurements were transmitted to the control subsystem, where they were compared with the preset desired tillage depth. The system then generates two deviation signals, *e1* and *e2*, representing the discrepancy between the actual and desired tillage depth values (Jin et al., 2020).

The LADRC employs linear state error feedback control laws to facilitate real-time adaptive adjustments to the hybrid stepper motor on a rotary tiller sliding platform based on the deviation signals, thereby enabling precise regulation of tillage depth changes. This adaptive adjustment mechanism allows the rotary-tiller system to effectively mitigate the impacts of uneven surfaces, shocks, and vibrations from the tilling environment, thus enabling more stable and precise tillage depth control.

Simulation of the adaptive LADRC tillage depth control system

A LADRC model was developed in MATLAB Simulink 2023a software based on the adaptive LADRC control method for tillage depth. The resulting model is illustrated in Figure 9. In the simulation, step-response experiments were conducted with preset tillage depths of 80 *mm* and 100 *mm*. The step responses are shown in Figure 10.

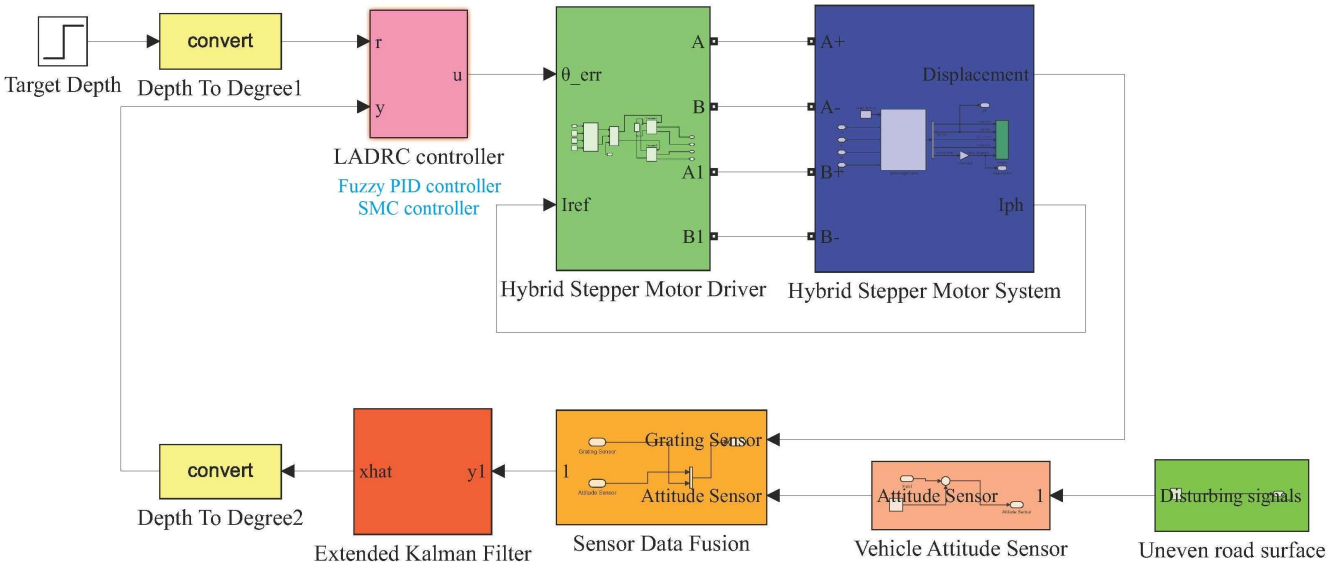

FIGURE 9. Simulation model of the LADRC controller.

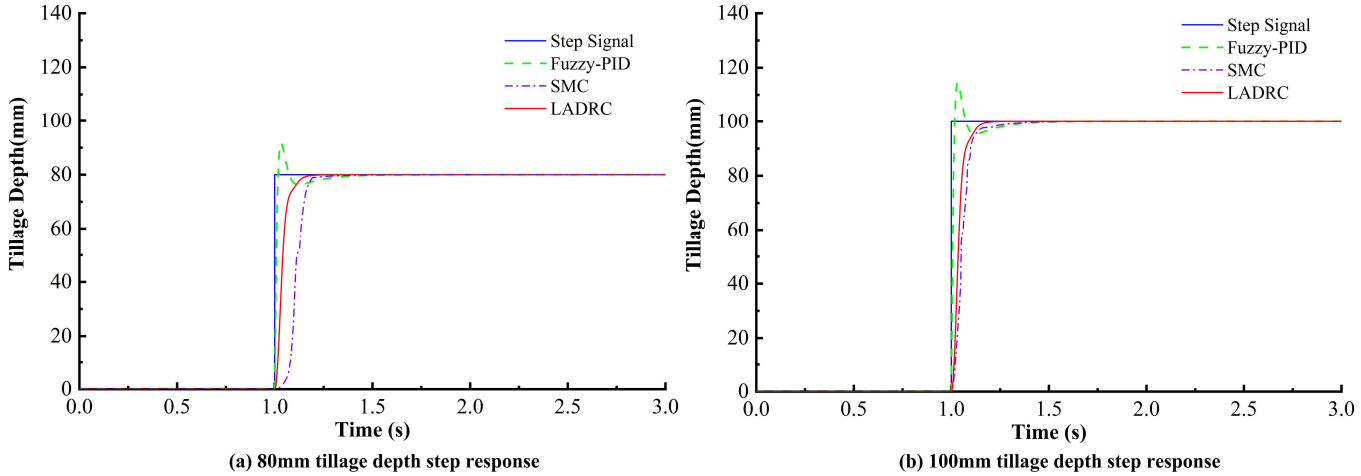

FIGURE 10. Step response plots for different tillage depths.

As illustrated in Figure 10, the LADRC shows superior response speed compared to the fuzzy PID and SMC controllers. The adjustment time was reduced by 46.4% in comparison with the fuzzy PID controller, with the LADRC showing no overshoot. The regulation time was reduced by 33.4% compared to the SMC controller. A comprehensive comparison of the results is presented in Table 2.

TABLE 2. Performance comparison of different controllers and tillage depth step response.

Tillage Depth(*mm*)	Controller Type	Adjustment Time(*s*)	Overshoot(%)
80	LADRC	0.135	0
80	SMC	0.189	0
80	Fuzzy-PID	0.252	16.3
100	LADRC	0.136	0
100	SMC	0.220	0
100	Fuzzy-PID	0.253	13.5

As illustrated in Figure 11, the random road unevenness is characterized by a maximum of 50.0 *mm* above the reference tillage depth level and a minimum of -18.0 *mm* below. Simulation experiments were conducted at preset tillage depths of 80 *mm* and 100 *mm*, and the control effects were compared with those of the fuzzy PID controller (see Figure 12). As illustrated in Figure 12, the tillage depth regulated by the LADRC demonstrated superior tracking performance. Compared with the fuzzy PID controller, the LADRC demonstrated a reduction in the magnitude of errors in the context of real-time dynamic tillage depth control. LADRC also outperformed SMC in terms of control performance, with smaller errors and better follow-up performance. The LADRC exhibited excellent real-time depth control performance, even when operating under uneven road conditions and in the presence of other disturbances.

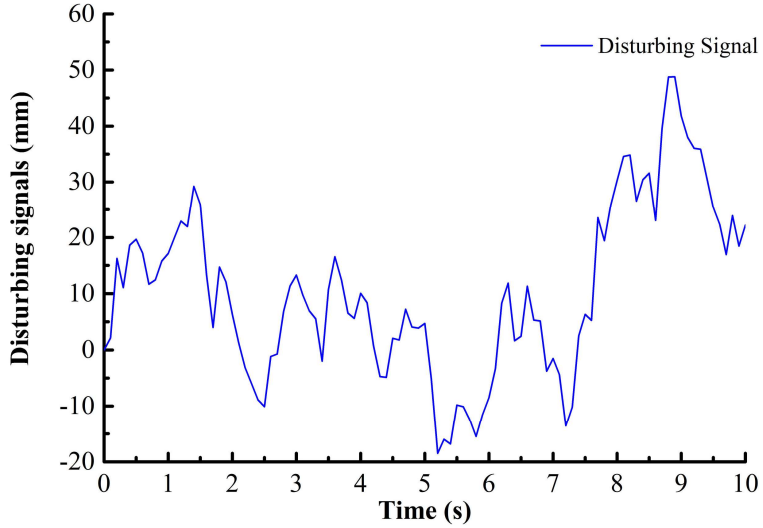

FIGURE 11. Randomized Road Disturbance Signal of Unevenness.

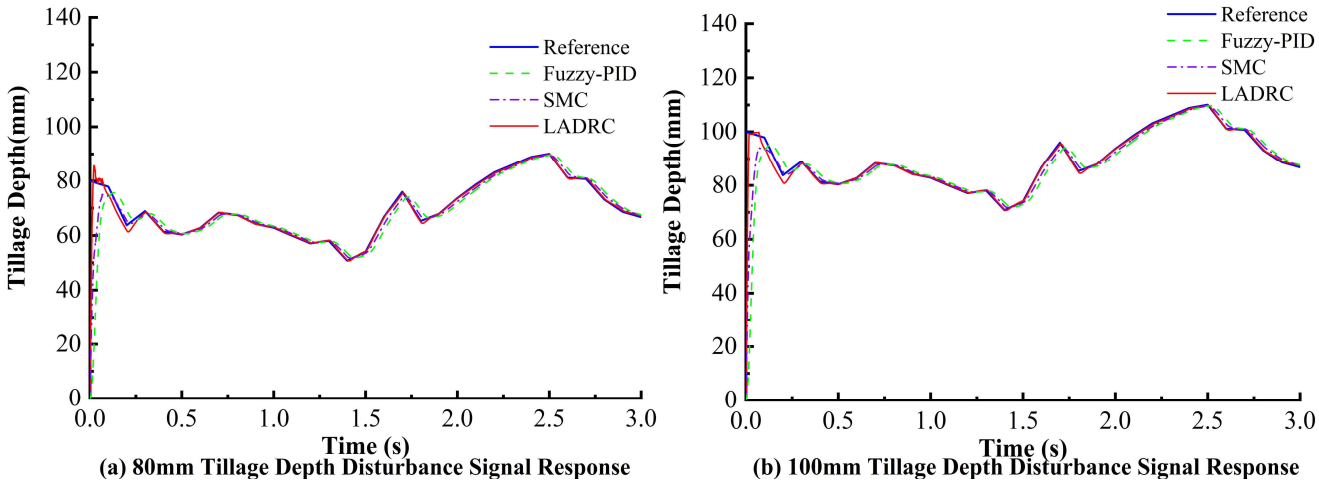

FIGURE 12. Performance of real-time control of different tillage depths under disturbing signals.

Tillage Depth Control System Experiment in Oolong Tea Plantations

Experimental method

Fuzzy PID, SMC, and LADRC control systems were employed to regulate the rotary-tilling depth of an electric rotary tiller under varying operational conditions. The efficacy of the three control strategies in the automatic tillage depth control systems was subsequently assessed. The uniformity and stability of rotary tillage under each control mode were assessed to determine with the required precision standards (Kim et al., 2021; Liu et al., 2023b).

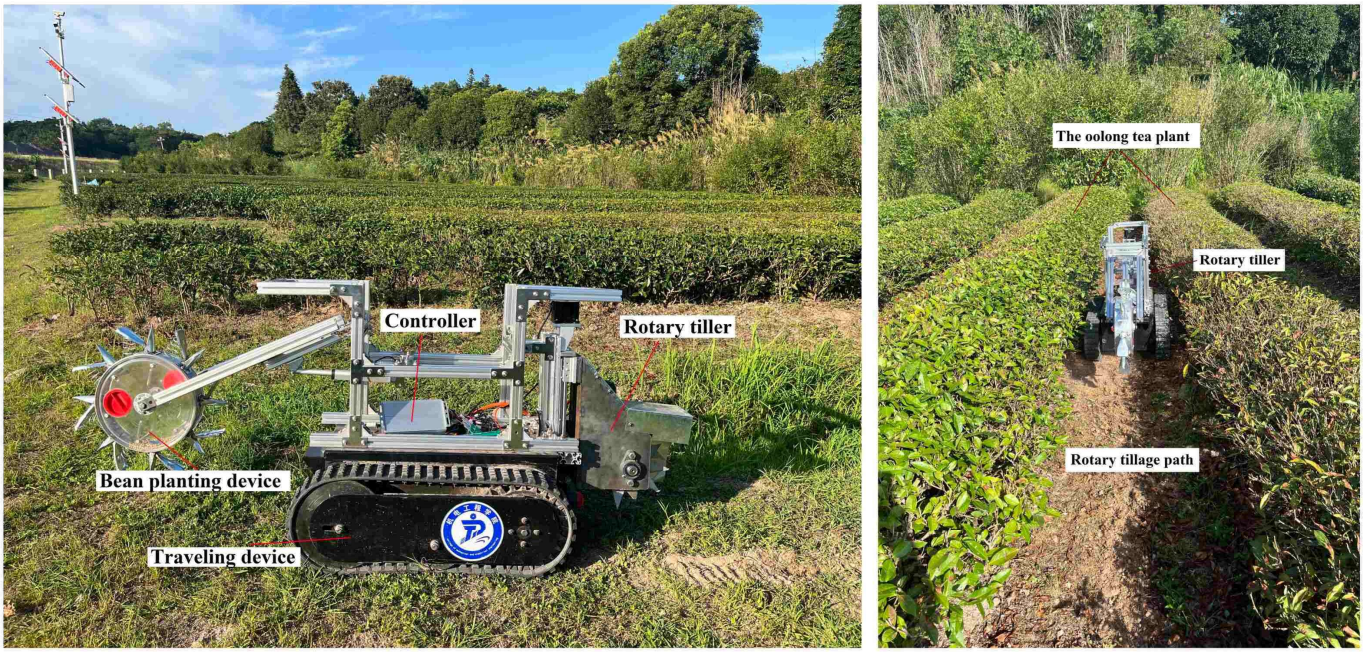

FIGURE 13. Electric Tiller Working Experiment.

As illustrated in Figure 13, electric rotary tillers are primarily used for intercropping tea trees and soybeans in tea plantations. The length of the test tea plantation was 20 *m*, and the average rotary speed of the rotary tiller was set to 150 *r/min* (Chen et al., 2021). Due to the lightweight and low-power design of the electric rotary tiller, the rotary speed may exceed the optimal range, resulting in potential slippage of the tiller. Furthermore, an excessive tillage depth may have contributed to this phenomenon. Incomplete tillage operations and other abnormal operating conditions may also occur. To mitigate these risks, two average operating speeds were tested: 0.5 *km/h* and 0.8 *km/h*. The recommended planting depth for soybeans is 50 *mm*, while the ideal soil tillage depth ranges between 80 and 100 *mm*. Therefore, the preset tillage depths were set at 80 *mm* and 100 *mm* for each operating speed, leading to four test conditions outlined in Table 3.

TABLE 3. Combination of test conditions of the tiller.

Working condition number Target tillage depth/mm Working speed/km·h-1	Target tillage depth/mm	Working speed/km·h^{-1}
1	80	0.5
2	100	0.5
3	80	0.8
4	100	0.8

The tillage-depth adjustment system was tested under these four operating conditions. Furthermore, the rotary tiller was considered stable within a 20 *m* test zone, with an additional 5 *m* on either side required to reach the desired tillage depth. Each experiment was repeated three times under different operating conditions, and the average value was recorded as the final result. The micro tiller was tested using two control systems: LADRC, SMC, and fuzzy PID. The following tests were conducted independently:

1. The machine status was verified to ensure that the control, walking, and rotary-tiller systems operated correctly.
2. Configure the fuzzy PID control algorithm, SMC control algorithm, or LADRC algorithm.
3. The timer was started, allowing the electric rotary tiller to begin operation, and the tiller unit was adjusted to reach the target depth.
4. Sampling points at 25 cm intervals along the path of the rotary tiller, and a total of 40 sampling points were selected.
5. Once the electric rotary tiller completed its operation, the actual tillage depth at the marked points was measured manually.

Experimental results and analysis

Experiments were conducted following the outlined methodology, and the results are shown in Fig. 14. The figure displays tillage depth values at each marked point under varying working conditions. The tillage depth curves for different working conditions after organizing the data are shown in Figure 15.

FIGURE 14. Data collection on the depth of rotary tillage.

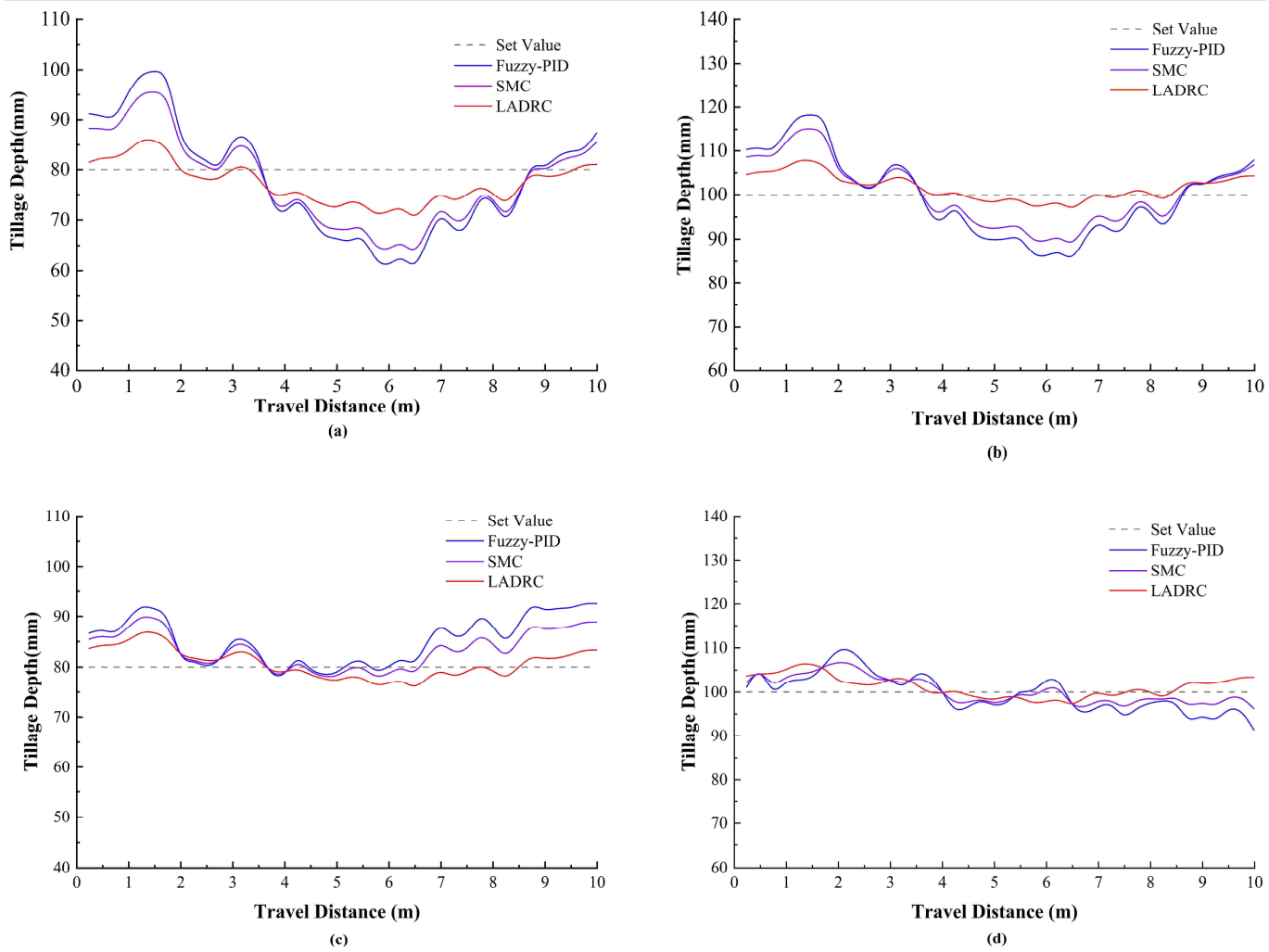

FIGURE 15. Rotary tillage depth under different control methods.

The experimental results demonstrated that fluctuations throughout the rotary-tilling process remained within a stable range. The outcomes varied based on specific working conditions, including the preset tillage depth and operating speed. As shown in Figure 15 and Table 4, the self-propelled electric rotary tiller employing fuzzy PID, SMC, and LADRC rapidly attained the desired tillage depth during actual operations. As illustrated in Figure 15, the maximum discrepancy between the actual and preset tillage depths across diverse operational conditions was 23 *mm*, while the minimum discrepancy was 16 *mm*. The mean standard deviation of the tillage depth was 3.2 *mm*, and the mean coefficient of variation in the tillage depth stability was 3.7%. The maximum deviation between the actual and preset tillage depths under different working conditions was 8 *mm* when the LADRC method was employed, with a minimum deviation of 6 *mm*. The mean standard deviations of the tillage depth, as measured using the SMC and Fuzzy PID control strategies, were 5.9 mm and 10.5 mm, respectively. Similarly, the mean coefficients of variation in tillage depth stability were 6.7% and 11.9%, respectively. The coefficient of variation of the tillage depth stability of the LADRC was reduced by 44.8% compared with that of the SMC. However, compared with the fuzzy-PID control method, the coefficient of variation of the depth of tillage stability for the LADRC strategy decreased even more, reaching 68.9%. Furthermore, the LADRC-based rotary-tiller equipment significantly reduced fluctuations in tillage depth while maintaining stability. This led to a reduction in the rate of tillage depth variation and an enhancement in the quality of rotary-tillage operations.

TABLE 4. Performance parameters of tillage depth for different control strategies.

No.	Control method	Working speed (km/h)	Target tillage depth (mm)	Average tillage depth (mm)	Standard deviation of tillage depth (mm)	Tillage depth stability coefficient of variation (%)
1	Fuzzy PID	0.5	80	77.8	11.2	14.4
2	SMC	0.5	80	77.7	9.1	11.7
3	LADRC	0.5	80	80.4	4.3	5.3
4	Fuzzy PID	0.5	100	97.7	9.5	9.7
5	SMC	0.5	100	103.7	7.5	7.2
6	LADRC	0.5	100	100.7	3.0	3.0
7	Fuzzy PID	0.8	80	83.1	10.6	12.8
8	SMC	0.8	80	82.4	3.9	4.7
9	LADRC	0.8	80	79.7	3.1	3.9
10	Fuzzy PID	0.8	100	97.9	10.5	10.7
11	SMC	0.8	100	98.7	3.2	3.2
12	LADRC	0.8	100	100.2	2.6	2.6

To verify the stability of the field test results, multiple experiments were conducted across multiple tea gardens. The soil hardness was assessed using a soil firmness testing instrument (model: IN-JSD-3) from AIYIN TEST, as shown in Figure 16. Most tea gardens exhibited soil hardness values ranging from 50 MPa to 150 MPa. The data from 500 field experiments were compiled to construct an error probability distribution curve (Fig. 17). Notably, the error distribution of the LADRC method was the most concentrated, with its peak centered at approximately 0°, indicating its exceptional reliability, robustness, and superior anti-interference performance.

As shown in Table 5, a quantitative analysis of the cost and energy consumption of the LADRC system was performed. The overall cost of the tillage depth control system was $172.27, keeping it below $200. The overall energy consumption of the system is approximately 100 W, demonstrating its energy-saving advantage. These factors indicate that the system demonstrates strong economic viability across a wide range of practical applications.

FIGURE 16. The soil firmness tester.

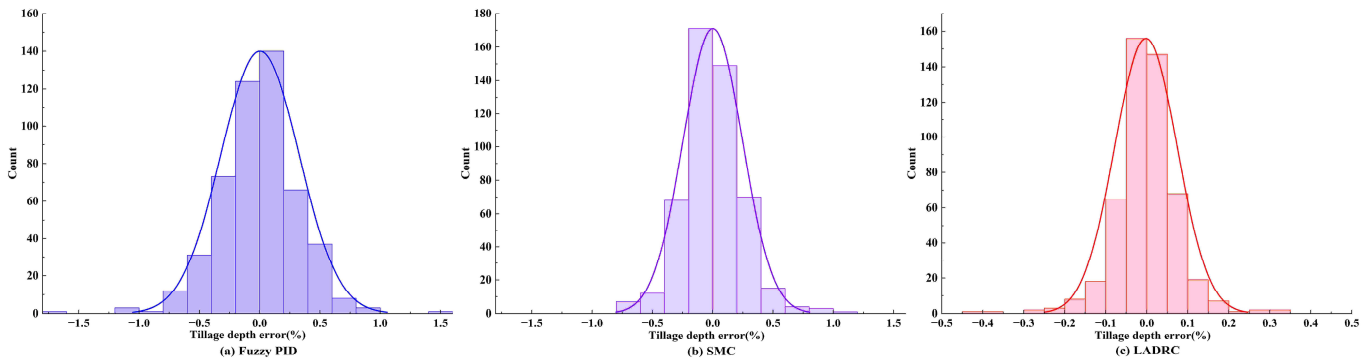

FIGURE 17. Error probability distribution curves of different control strategies.

TABLE 5. Tillage control system costs and energy consumption statistics.

Items		Price/Energy consumption
Hardware Costs	Controllers	$1.63
	Sensors	$22.48
	Actuators	$60.74
	Other Modules	$27.42
Software Costs	System Integration	$30.0
	System Testing	$30.0
Overall cost of the tillage control system		$172.27
Energy consumption	Controller Energy Consumption	0.33~1.0 W
	Sensor energy consumption	0.25~1.0 W
	Actuator energy consumption	90~100 W
Overall system energy consumption		90.58~102 W

CONCLUSIONS

This paper proposes a novel tillage depth control system incorporating body posture sensors, grating sensors, control units, and hybrid stepper motors, with the aim of addressing the issue of uneven tillage depth control in electric rotary tillers. The STM32 microcontroller served as the control unit, and the LADRC strategy was innovatively applied to a tillage depth control system. The system achieves a control response time of 0.14 s, ensuring high precision, rapid response speed, and minimal fluctuation in tillage depth control. An electric rotary tiller utilizing the LADRC strategy is capable of maintaining stable tillage depth throughout the operational cycle. Compared to the fuzzy PID and SMC controls, the LADRC strategy demonstrated a 68.9% reduction in the variation in tillage depth stability, thereby meeting the consistency requirements for tillage depth. The system achieved a fully adaptive closed-loop control process for the tillage depth by collecting real-time signals from the grating sensor and comparing the actual tillage depth with the target value. This control system is highly practical and has significant value in research on tillage depth control in electric rotary tillers. However, the selection of LADRC parameters, such as bandwidth and gain, relies on experimental experience. Future work will further explore the use of optimization methods such as particle swarm optimization (PSO) and deep learning to adaptively select LADRC parameters, thereby enhancing the adaptability of the system.

Funding: This research was funded by the Natural Science Foundation of Fujian Province (grant nos. 2022J011191 and 2024J01909), the Fujian Provincial Technological Innovation Key Research and Industrialization Projects (grant no. 2024XQ024), Wuyi University Horizontal Project (grant no. 2024-WHFW-030), and the Nanping Science and Technology Plan Project (grant nos. N2023Z001, N2023Z002, N2023J001 and N2024Z001).

Author Contributions: Conceptualization, Wei Tao and Bin Chen; Methodology, Wei Tao; Software, Wei Tao and Bin Chen; Validation, Bin Chen and Shaoye Ke; Data Curation, Shenghong Huang; Writing—Original Draft Preparation, Bin Chen; Writing—Review and Editing, Wei Tao.

Conflicts of Interest: The authors declare no conflict of interest.

REFERENCES

Chen P., Tao, W., Zhu, L., Wu, Q.-M., & Zhang, J.-W. (2021). Effect of varying remote cylinder speeds on plough-breast performances in alternative shifting tillage. *Computers Electronics in Agriculture, 181*, 105963. https://doi.org/10.1016/j.compag.2020.105963

Fawzi, H., Mostafa, S. A., Ahmed, D., Alduais, N., & Mohammed, M. A. (2021). TOQO: A new Tillage Operations Quality Optimization model based on parallel and dynamic Decision Support System. *Journal of Cleaner Production, 316*, 128263. https://doi.org/10.1016/j.jclepro.2021.128263

Gao, Z. (2003). *Scaling and bandwidth-parameterization based controller tuning*. In Proceedings of the 2003 American Control Conference (pp. 4993). Denver, CO, USA.

Gao, Z. Yan, H., & Zhou, X. (2024). *Active Disturbance Rejection Control of Microgrid DC-DC Converter Based on AC Algorithm.* Paper presented at the 2024 IEEE International Conference on Mechatronics and Automation (ICMA).

Groenhuis, V., Rolff, G., Bosman, K., Abelmann, L., & Stramigioli, S. (2021). Multi-axis electric stepper motor. *IEEE Robotics automation letters 6*(4), 7201-7208. https://doi.org/10.1109/LRA.2021.3097077

Han, J.-Q. (1999). Nonlinear design methods for control systems. *IFAC Proceedings Volumes, 32*(2), 1531-1536. https://doi.org/10.1016/S1474-6670(17)56259-X

Han, J. (2009). From PID to active disturbance rejection control. *IEEE Transactions on Industrial Electronics, 56*(3), 900 - 906. https://doi.org/10.1109/TIE.2008.2011621

Hojati, M., Baktash, A., & Mukhopadhyay, S. C (2024). Investigation of torque and sensitivity analysis of a two-phase hybrid stepper motor. *International Journal on Smart Sensing Intelligent Systems, 17*(1). https://doi.org/10.2478/ijssis-2024-0020

Hu, K., Zhang, W., Qi, B., & Ji, Y. (2024). Tillage depth dynamic monitoring and precise control system. *Measurement Control* 0(0). https://doi.org/10.1177/00202940241263454

Jia, H., Guo, M., Yu, H., Li, Y., & Feng, X. (2016). An adaptable tillage depth monitoring system for tillage machine. *Biosystems Engineering, 151*, 187-199. https://doi.org/10.1016/j.biosystemseng.2016.08.022

Jin, H., Song, J., Lan, W., & Gao, Z. (2020) On the characteristics of ADRC: A PID interpretation. *Science China. Information Sciences, 63*(10), 209201. https://doi.org/10.1007/s11432-018-9647-6

Kim, Y.-S., Kim, T.-J., Kim, Y.-J., Lee, S.-D., & Park, S.-U. (2020). Development of a real-time tillage depth measurement system for agricultural tractors: application to the effect analysis of tillage depth on draft force during plow tillage. *Sensors, 20*(3), 912. https://doi.org/10.3390/s20030912

Kim, Y.-S., Lee, S.-D., Baek, S.-M., Baek, S.-Y., & Jeon, H.-H. (2022). Analysis of the effect of tillage depth on the working performance of tractor-moldboard plow system under various field environments. *Sensors, 22*(7), 2750. https://doi.org/10.3390/s22072750

Kim, Y.-S., Siddique, M. A. A., Kim, W.-S., Kim, Y.-J., & Lee, S.-D. (2021). DEM simulation for draft force prediction of moldboard plow according to the tillage depth in cohesive soil. *Computers Electronics in Agriculture, 189*, 106368. https://doi.org/10.1016/j.compag.2021.106368

Li, H., Hu, X., & Cui, L. (2023). Magnetic field analysis for the permanent magnet spherical motor with SMC core. *IEEE Transactions on Magnetics, 59*(6), 1-9. https://doi.org/10.1109/TMAG.2023.3244617

Liu, C., Yang, K., Chen, Y., Gong, H., & Feng, X. (2023a). Benefits of mechanical weeding for weed control, rice growth characteristics and yield in paddy fields. *Field Crops Research, 293*, 108852. https://doi.org/10.1016/j.fcr.2023.108852

Liu, G., Zheng, K., Xia, J., Cheng, J., & Liu, Z. (2024b). Research on an intelligent vibration detachment system for rotary tiller based on soil surface roughness dynamic characteristics. *Computers Electronics in Agriculture, 224*, 109214. https://doi.org/10.1016/j.compag.2024.109214

Liu, K., Sozzi, M., Gasparini, F., Marinello, F., & Sartori, L. (2023b). Combining simulations and field experiments: Effects of subsoiling angle and tillage depth on soil structure and energy requirements. *Computers Electronics in Agriculture, 214*, 108323. https://doi.org/10.1016/j.compag.2023.108323

Liu, W., Yang, R., Li, L., Zhao, C., & Li, G. (2024a). Energy and environmental evaluation and comparison of a diesel-electric hybrid tractor, a conventional tractor, and a hillside mini-tiller using the life cycle assessment method. *Journal of Cleaner Production, 469*, 143232. https://doi.org/10.1016/j.jclepro.2024.143232

Luo, C., Wen, C., Meng, Z., Liu, H., & Li, G. (2023). Research on the slip rate control of a power shift tractor based on wheel speed and tillage depth adjustment. *Agronomy, 13*(2), 281. https://doi.org/10.3390/agronomy13020281

Sabouri, Y., Abbaspour-Gilandeh, Y., Solhjou, A., Shaker, M., & Szymanek, M. (2021). Development and laboratory evaluation of an online controlling algorithm for precision tillage. *Sensors, 21*(16), 5603. https://doi.org/10.3390/s21165603

Sahoo, A. U., Raheman, H. (2020). Development of an electric reaper: a clean harvesting machine for cereal crops. *Clean Technologies Environmental Policy, 22*, 955-964. https://doi.org/10.1007/s10098-020-01838-7

Wang, A., Ji, X., Zhu, Y., Wang, Q., & Wei, X. (2024). Tillage depth regulation system via depth measurement feedback and composite sliding mode control: A field comparison validation study. *Measurement Control, 57*(6), 685-702. https://doi.org/10.1177/00202940231216139

Wang, Q., Wang, X., Wang, W., Song, Y., & Cui, Y. (2023). Joint control method based on speed and slip rate switching in plowing operation of wheeled electric tractor equipped with sliding battery pack. *Computers and Electronics in Agriculture, 215*, 108426. https://doi.org/10.1016/j.compag.2023.108426

Wu, S., Shi, T., Guo, L., Wang, H., & Xia, C. (2020) Accurate analytical method for magnetic field calculation of interior PM motors. *IEEE Transactions on Energy Conversion, 36*(1), 325-337. https://doi.org/10.1109/TEC.2020.3000753

Xiao, M., Ma, Y., Wang, C., Chen, J., & Zhu, Y. (2023). Design and experiment of fuzzy-PID based tillage depth control system for a self-propelled electric tiller. *International Journal of Agricultural Biological Engineering, 16*(4), 116 - 125. https://doi.org/10.25165/j.ijabe.20231604.8116